Article:
Nakiganda, AM orcid.org/0000-0003-3017-5525, Dehghan, S, Markovic, U et al. (2 more authors) (2022) A Stochastic-Robust Approach for Resilient Microgrid Investment Planning Under Static and Transient Islanding Security Constraints. IEEE Transactions on Smart Grid, 13 (3). pp. 1774-1788. ISSN 1949-3053

https://doi.org/10.1109/tsg.2022.3146193

A Stochastic-Robust Approach for Resilient Microgrid Investment Planning Under Static and Transient Islanding Security Constraints

Agnes Marjorie Nakiganda, *Student Member, IEEE,* Shahab Dehghan, *Senior Member, IEEE,* Uros Markovic, *Member, IEEE,* Gabriela Hug, *Senior Member, IEEE,* and Petros Aristidou, *Senior Member, IEEE*

***Abstract*—When planning the investment in Microgrids (MGs), usually static security constraints are included to ensure their resilience and ability to operate in islanded mode. However, unscheduled islanding events may trigger cascading disconnections of Distributed Energy Resources (DERs) inside the MG due to the transient response, leading to a partial or full loss of load. In this paper, a min-max-min, hybrid, stochastic-robust investment planning model is proposed to obtain a resilient MG considering both High-Impact-Low-Frequency (HILF) and Low-Impact-High-Frequency (LIHF) uncertainties. The HILF uncertainty pertains to the unscheduled islanding of the MG after a disastrous event, and the LIHF uncertainty relates to correlated loads and DER generation, characterized by a set of scenarios. The MG resilience under both types of uncertainty is ensured by incorporating static and transient islanding constraints into the proposed investment model. The inclusion of transient response constraints leads to a min-max-min problem with a non-linear dynamic frequency response model that cannot be solved directly by available optimization tools. Thus, in this paper, a three-stage solution approach is proposed to find the optimal investment plan. The performance of the proposed algorithm is tested on the CIGRE 18-node distribution network.**

***Index Terms*—Investment planning, microgrids, low-inertia, frequency constraints, unscheduled islanding, resilience.**

NOMENCLATURE

Functions

$\Theta^{\mathrm{gm,opr}}$	Total operational costs in grid-connected mode [$].
$\Theta^{\mathrm{im,opr}}_{to}$	Total penalty costs of disconnecting loads from MG at hour t in representative day o in islanded mode [$].
$\breve{\Theta}^{\mathrm{im,opr}}$	Vector-valued function of total penalty costs of disconnecting loads from MG in islanded mode [$].
Θ^{inv}	Total investment costs [$].

Indices

g	Index of generators, $g \in \{c, d, i, v\}$.
n	Index of nodes, n''/n' being a node before/after node n.
o	Index of representative days.
t	Index of hours.
ψ	Index of iterations.

Parameters

c_{go}	Daily capacity factor of generator g in representative day o.
D	Normalized damping constant of all generators [p.u.].
D_i	Damping constant of Synchronous Generators (SGs), D_s is the weighted average of all SGs [p.u.].
D_v	Virtual damping constant of Virtual Synchronous Machine (VSM) based Converter-Interfaced Generators (CIGs) v, D_c is the weighted average of all CIGs [p.u.].
$d^{\mathrm{p_c/q_c}}_{nto}$	Constant part of active/reactive load power [kW/kVAr].
e_{no}	Flexible energy demand of node n in representative day o [kWh].
$e^{\mathrm{b/s}}_{to}$	Buying/selling price of electricity from/to the main grid at hour t in representative day o [$/kWh].
e^{FR}_{g}	Minimum reserve energy capacity for transient frequency response of generator g [kWh].
F_i	Fraction of the total power generated by the turbine of SG i, F_s being the weighted average of all SGs [p.u.].
fc_n	Penalty cost of shifting demand at node n [$/kWh].
ic_g	Annualized investment cost of generator g [$].
$ic_{nn'}$	Annualized investment/reinforcement cost of a line connecting nodes (n, n') [$].
K_d	Power gain factor of droop-based CIG d [p.u.].
K_i	Mechanical power gain factor of SG i [p.u.].
M	Normalized inertia constant of all SGs and CIGs [s].
M_s	Normalized inertia constant for the Center-of-Inertia (CoI) of SGs [s].
M_v	Virtual inertia constant of CIG v with VSM control, M_c is the normalized inertia of all CIGs [s].
mc_g	Marginal cost of generator g [$/kWh].
pc_n	Penalty cost of disconnecting demand at node n [$/kWh].
p^{AV}_{gto}	Maximum available power for CIG unit g at hour t in representative day o [kW].
p^{FR}_{g}	Minimum reserve power capacity for transient frequency response of generator g [kW].
p^{nom}_{g}	Nominal capacity of CIG and SG g [kW].
R_d	Droop of CIG d with droop control, R_c being the weighted average of all CIGs [%].
R_i	Droop of SG i, R_s being the weighted average of all SGs [%].
$r^{\mathrm{d/u}}_{g}$	Ramp-down/ramp-up limit of generator g [kW/h].
$r_{n'n}$	Resistance of the line connecting nodes (n, n') [Ω].
$x_{n'n}$	Reactance of the line connecting nodes (n, n') [Ω].
$\overline{s}_{n'n}$	Capacity of the line connecting nodes (n, n') [kVA].
$T_{d/v}$	Time constant of CIG with droop/VSM control [s].
T_i	Turbine time constant of SG i [s].

A. Nakiganda is with the School of Electronic and Electrical Engineering, University of Leeds, UK.

S. Dehghan is with the Department of Electrical and Electronic Engineering, Imperial College London, UK.

U. Markovic and G. Hug are with the Power Systems Laboratory, ETH Zurich, Switzerland.

P. Aristidou is with the Department of Electrical Engineering and Computer Engineering and Informatics, Cyprus University of Technology, Cyprus. Email: el14amn@leeds.ac.uk.

This work was partially supported by the Engineering and Physical Sciences Research Council (EPSRC) in the UK under grant reference EP/R030243/1.

$z^0_{nn'}$ Initial status of a line connecting nodes (n, n') (i.e., $1/0$: built/not-built).
α Scaling factor.
ζ Damping ratio.
ω_n Natural frequency [Hz].
τ_o Weighting factor of representative day o.
ϵ Corrective power deviation tolerance [kW].

Sets

Ω^{C} Set of CIGs, $\Omega^{\mathrm{C_n}}$ being the set of generators connected to node n.
$\Omega^{\mathrm{C}}_{d/v}$ Set of CIGs with droop/VSM control scheme.
$\Omega^{\mathrm{gm,opr}}$ Feasible space of operational variables in grid-connected mode.
$\Omega^{\mathrm{im,opr}}$ Feasible space of operational variables in islanded mode.
Ω^{inv} Feasible space of investment-related variables.
Ω^{L} Set of lines connecting neighbouring nodes.
Ω^{MG} Feasible space of the MG planning problem.
Ω^{N} Set of nodes, $\Omega^{\mathrm{N_n}}$ being the set of nodes after and connected to node n.
Ω^{O} Set of representative days.
Ω^{S} Set of SGs, $\Omega^{\mathrm{S_n}}$ being the set of generators connected to node n.
Ω^{T} Set of hours in a representative day.

Symbols

$\hat{\bullet}$ Deviations of the quantity $\bullet$ in the islanded mode from its value in the grid-connected mode (i.e., $\hat{d}^{\mathrm{p_f}}_{nto}$ and $\hat{d}^{\mathrm{q_f}}_{nto}$), $\hat{\bullet}^{+}/\hat{\bullet}^{-}$ being upward/downward deviations (i.e., $\hat{d}^{\mathrm{p_f}^{+}}_{nto}$, $\hat{d}^{\mathrm{p_f}^{-}}_{nto}$, $\hat{d}^{\mathrm{q_f}^{+}}_{nto}$, and $\hat{d}^{\mathrm{q_f}^{-}}_{nto}$).
$|\bullet|$ Cardinality of the set $\bullet$.
$\underline{\bullet}/\overline{\bullet}$ Lower/upper bounds of the quantity $\bullet$.

Variables

$d^{\mathrm{p/q}}_{nto}$ Active/reactive load power at node n, hour t, and representative day o [kW/kVAr].
$d^{\mathrm{p_f/q_f}}_{nto}$ Flexible part of active/reactive load power at node n, hour t, and representative day o [kW/kVAr].
p/q_{gto} Active/reactive power generation of generator g at hour t and representative day o [kW/kVAr].
$p/q^{\mathrm{b/s}}_{to}$ Active/reactive power flow bought/sold to the main grid at hour t and representative day o [kW/kVAr].
$p_{nn'to}$ Active power flow of a line connecting nodes (n, n') at hour t and representative day o [kW].
$q_{nn'to}$ Reactive power flow of a line connecting nodes (n, n') at hour t and representative day o [kVAr].
v_{nto} Voltage magnitude at node n, hour t, and representative day o [V].
y_{nto} Binary variable indicating the connection status of load at node n, hour t, and representative day o (i.e., $1/0$: connected/disconnected).
z_g Binary variable indicating the investment status of generator g (i.e., $1/0$: built/not-built).
$z_{nn'}$ Binary variable indicating the investment/reinforcement status of a line connecting nodes (n, n') (i.e., $1/0$: built/not-built).

Vectors

χ Vector of all investment and operational variables.
$\chi^{\mathrm{gm,opr}}$ Vector of "wait-and-see" operational variables in grid-connected mode.
$\chi^{\mathrm{im,opr}}$ Vector of "wait-and-see" operational variables in islanded mode.
χ^{inv} Vector of "here-and-now" investment variables.
η Vector of representative days (i.e., scenarios).

I. Introduction

Resilient electric networks must have the ability to ride through extreme contingencies, maintain basic service levels to critical load demands, and ensure fast recovery to normality. In other words, a resilient system should be able to modify its functionality and alter its structure in an agile manner without collapsing [1]. The main measures to enhance the resilience of electric networks can be categorized into [2]: (i) *"hardening"*, which incorporates all activities aimed at reinforcing electric networks and enhancing component designs and constructions with the intention of preserving functionality and minimizing damage; (ii) *"survivability"*, which includes innovative technologies to diversify energy supply and improve system flexibility; and (iii) *"recovery"*, which incorporates all tools aimed at restoring the system to normal operating conditions. Of particular concern is the resilience of electricity distribution networks due to their interdependence with other critical infrastructure, which might culminate in a sustained negative impact on society. With this background, Microgrids (MGs) have been widely considered as a potential pathway for enhancing system resilience and ensuring both structural reinforcement and operational flexibility by allowing for the coexistence of Distributed Energy Resources (DERs) with the traditional bulk grid [3], [4].

MG, as defined in [5], refers to "*a group of interconnected loads and distributed energy resources with clearly defined electrical boundaries that acts as a single controllable entity with respect to the grid and can connect and disconnect from the grid to enable it to operate in both grid-connected or island modes*". Their islanding capability is critical in enhancing resilience by ensuring continuity and mitigating interruptions of energy supply to consumers in the event of extreme weather conditions or significant faults in the bulk transmission grid [6], [7]. The successful island creation, especially following disastrous events, is subject to the secure transient performance of DERs, thus ensuring the survivability of the MG. However, unlike traditional bulk grids, MGs are inherently faced with a lack of rotational inertia and damping capability affecting their security in the event of significant power imbalance, and more importantly, islanding from the main grid [8], [9]. A MG is considered secure if all equipment (e.g., lines and generators) operate within their technical limits and tolerances avoiding subsequent network disconnections and associated risk of cascading failures [10]. Thus, it is vital to design a resilient and reliable MG able to withstand both High-Impact-Low-Frequency (HILF) and Low-Impact-High-Frequency (LIHF) uncertainties, under static and transient operational constraints. On the one hand, static islanding constraints ensure the MG's operational adequacy in supplying the forecasted electricity demand. On the other hand, transient islanding constraints ensure the MG's operational security by adhering to a dynamic response within the defined regulatory limits and, consequently, avoiding the operation of protective devices that would result in DER disconnections.

Different planning tools including: stochastic [11], robust [12]–[15], and distributionally robust [16] approaches have been previously presented in the literature for optimal investment

in distribution networks and MGs aiming at enhancing system resilience to extreme contingencies. In [11], a stochastic model has been proposed for optimal investment in distribution networks under different disastrous events characterized by a set of scenarios. In [12], a robust resilience-constrained MG planning model is introduced under the uncertainty of loads and power generation of Renewable Energy Sources (RESs), with islanding from the main grid considered as another source of uncertainty. In [13], a robust defender-attacker-defender model is presented for optimal hardening planning in resilient distribution networks, considering topology reconfiguration and islanding formation. Besides, in [15], a robust model is proposed for hardening and investment planning in distribution networks based on a multi-stage and multi-zone uncertainty modeling of spatial and temporal characteristics of natural disasters. Additionally, a distributionally robust resilience-constrained investment planning model under natural disasters is introduced in [16], where a moment-based ambiguity set characterizes extreme events. Even though the literature offers several operational planning models for traditional bulk grids under dynamic security constraints [17]–[23], to the best of the authors' knowledge, previous resilience-constrained investment planning models for MGs [12], [24], and even active distribution networks [11]–[13], [15], have only considered static operational constraints rather than dynamic.

In [25], static frequency security for primary, secondary and tertiary control levels in MGs has been studied, however, transient frequency security was not considered. The problem of ensuring transient security in power systems has been studied in [17], where a transient stability-constrained Optimal Power Flow (OPF) is employed with a single-machine infinite-bus model characterizing the transient stability constraints in order to facilitate secure frequency response. Similarly, a discretized transient response is embedded in the OPF problem in [18] to ensure a secure transient frequency response. In [19], an analytical formulation is presented to limit the Rate-of-Change-of-Frequency (RoCoF) based on a single-machine CoI frequency model, while [20] uses a simplified model of transient frequency metrics to analyze the post-fault response. Such simplified frequency response models tend to describe system dynamics inaccurately and cannot quantify the support provided by different units. A reduced second-order model is used in [21] to determine sufficient synthetic inertia and droop slopes for a collection of traditional and inverter-interfaced generators that satisfy both steady-state and dynamic frequency requirements. Moreover, in [22] and [23], the unit commitment problem is solved under frequency-related constraints for traditional and low-inertia grids, where frequency-related constraints are derived based on a low-order non-linear frequency response model [26].

Nevertheless, all aforementioned studies have certain drawbacks, as they are based on either simplified dynamic models [19]–[21], linearized frequency-related constraints [22], or make *ex-ante* bound extractions on the relevant variables [23] to simplify the planning model. Furthermore, the simplifications therein represent the characteristic properties of transmission networks rather than active distribution networks and MGs. Accordingly, it is vital to present a resilience-oriented MG planning tool, including both static and transient constraints, based on a detailed dynamic model to ensure satisfactory operation given the abrupt main grid disconnection in the event of extreme contingencies.

The paper's main contributions can be summarized as follows:

- A min-max-min, stochastic-robust, investment planning model, is introduced to design a resilient MG under both HILF and LIHF uncertainties. The HILF uncertainty pertains to the unscheduled islanding of the MG from the main grid while the LIHF uncertainties relate to correlated load and RES generation. For the latter, the k-means clustering technique is used to obtain a sufficient number of scenarios (i.e., representative days) characterizing different realizations of LIHF uncertainties. The stochastic approach obtains an optimal solution over all LIHF scenarios while the robust approach immunizes each scenario (i.e., every hour of each representative day) against the power loss associated with the unscheduled islanding of the MG (i.e., HILF scenario) at an optimized cost.
- Both static and transient islanding constraints (i.e., the maximum RoCoF and the frequency nadir as transient-state criteria, and the frequency deviation as a quasi steady-state criterion) are considered in the proposed model to ensure resilience under HILF and LIHF uncertainties. To the best of the authors' knowledge, there is no similar planning tool in the literature that includes both static and transient islanding constraints.
- A tractable three-stage solution approach is presented since the proposed min-max-min, hybrid, stochastic-robust investment problem with a non-linear frequency response model cannot be solved directly.

The rest of the paper is organized as follows. In Section II, the investment planning model is described in a compact form together with the main modeling preliminaries. Section III presents the detailed problem formulation under static and transient islanding constraints, whereas Section IV discusses the application of the proposed investment planning model on the CIGRE 18-node distribution network in order to design a resilient MG under different operating conditions. Finally, Section V concludes the paper.

II. Modeling Preliminaries and Problem Description

In this paper, the uncertainty pertaining to the unscheduled islanding of the microgrid from the main grid is considered as HILF due to its severe impact on the microgrid brought about by the loss of a large power in/outfeed from/to the main grid and its low frequency of occurrence. In addition, uncertainties pertaining to load and renewable generation are considered as LIHF due to their low impacts on the amount of power exchange with the main grid and their high frequencies of occurrences. For instance, the load of the microgrid at each hour of a single day is a continuous uncertain parameter, and this uncertain parameter can be repeated $24 \times 365 = 8760$ times per year. On the contrary, a microgrid may face only a few unscheduled islandings per year. Therefore, the former is a high-frequency uncertainty while the later is a low-frequency one.

Both types of uncertainties have been considered in the proposed stochastic-robust model to enhance the resilience of the microgrid. In general, a stochastic approach finds a solution that is optimal on average for a set of scenarios characterizing uncertain parameters, while a robust approach finds a solution that is optimal for the worst-case realization of uncertain parameters. In this paper, a stochastic approach is utilized to characterize the uncertainty of load and renewable generation

by a set of scenarios, named as representative days. In addition, a robust approach is utilized to characterize the uncertainty of unscheduled islanding from the main grid. Note that the proposed approach considers the possibility of an islanding event for all hours of each representative day. Hence, it is robust against a disruptive event at all hours of each representative day.

The main modeling preliminaries in the proposed investment planning model are:

- Without loss of generality, a single-year planning horizon is considered rather than a multi-year one to reach a compromise between accuracy and tractability of the proposed model.
- To capture interday/intraday variation/ramping of uncertain loads and power generation of RESs, a sufficient number of representative days (i.e., *scenarios*) is considered, obtained by the k-means clustering technique [27].
- A single scheduling period of each representative day is considered to be *one hour* both in grid-connected and islanded modes.
- The MG is assumed to have a radial network topology, as such, a linearized version of the DistFlow model is used for the power flow formulation to obtain a linear optimization problem [28], [29]. Additionally, the quadratic line flow expressions are linearized using a piecewise linear approximation [30]. Finally, a constant marginal cost is utilized to eliminate the non-linearity of quadratic cost functions [27].
- It is assumed that an unscheduled islanding event might happen at *each* period of the representative days considered.
- After an islanding, a single period of islanded operation is assumed and the probability of further contingencies in the islanded mode is not considered.

A. Compact Formulation under Static Constraints

The proposed min-max-min investment planning model under static operational constraints in grid-connected and islanded mode can be presented in compact form as:

$$\min_{\chi\in\Omega^{\mathrm{MG}}} \; \Theta^{\mathrm{inv}}(\chi^{\mathrm{inv}}) + \Theta^{\mathrm{gm,opr}}(\chi^{\mathrm{inv}},\chi^{\mathrm{gm,opr}}) + ||\breve{\Theta}^{\mathrm{im,opr}}(\chi^{\mathrm{inv}},\chi^{\mathrm{gm,opr}},\chi^{\mathrm{im,opr}})||_{\infty}, \tag{1}$$

where $\Omega^{\mathrm{MG}} = \{\chi = [\chi^{\mathrm{inv}},\chi^{\mathrm{gm,opr}},\chi^{\mathrm{im,opr}}]\,|\,\chi^{\mathrm{inv}} \in \Omega^{\mathrm{inv}};\, \chi^{\mathrm{gm,opr}} \in \Omega^{\mathrm{gm,opr}};\, \chi^{\mathrm{im,opr}} \in \Omega^{\mathrm{im,opr}}\}$, $\breve{\Theta}^{\mathrm{im,opr}} = [\min\,\Theta^{\mathrm{im,opr}}_{11},...,\min\,\Theta^{\mathrm{im,opr}}_{\mathcal{TO}}]$, $\mathcal{T} = |\Omega^{\mathrm{T}}|$, and $\mathcal{O} = |\Omega^{\mathrm{O}}|$. Also, $||\breve{\Theta}^{\mathrm{im,opr}}||_{\infty} = \max(\min_{\forall t,\forall o} \Theta^{\mathrm{im,opr}}_{to})$. Hence, the objective function (1) minimizes the total investment costs (Θ^{inv}), the *"expected"* total operation costs in grid-connected mode for all hours of all representative days ($\Theta^{\mathrm{gm,opr}}$), and the *"worst-case"* total penalty costs of disconnecting loads from MG in islanded mode for all hours in all representative days ($\Theta^{\mathrm{im,opr}}$).

The min-max-min objective function (1) can be rewritten as a single minimization problem by using the auxiliary variable γ:

$$\min_{\chi\in\Omega^{\mathrm{MG}}} \; \Theta^{\mathrm{inv}}(\chi^{\mathrm{inv}}) + \Theta^{\mathrm{gm,opr}}(\chi^{\mathrm{inv}},\chi^{\mathrm{gm,opr}}) + \gamma \tag{2a}$$

$$\text{s.t.} \quad \gamma \geq \Theta^{\mathrm{im,opr}}_{to}(\chi^{\mathrm{inv}},\chi^{\mathrm{gm,opr}},\chi^{\mathrm{im,opr}}),\ \forall t\in\Omega^{\mathrm{T}}, o\in\Omega^{\mathrm{O}}, \tag{2b}$$

The optimization problem (2) is a Mixed-Integer Linear Programming (MILP) problem, and as such can be solved by available software packages to obtain optimal investment and operation decisions in grid-connected and islanded mode.

However, the operation decisions may violate transient islanding constraints. To remedy such limitation and ensure MG resilience before and after an islanding event, a non-linear model for evaluation of the transient frequency response of a MG after islanding can be incorporated. The resultant problem is a complicated Mixed-Integer Non Linear Programming (MINLP), non-convex problem that can be intractable in practical applications. A three-stage methodology that incorporates the transient frequency constraints through sequential linearization and iterative tightening of power bounds is thus employed. In the sequel, the MG frequency dynamics, the metrics to evaluate the transient frequency response of a MG in islanded mode, as well as the proposed three-stage solution approach are presented.

B. Microgrid Frequency Dynamics

The employed dynamic model in this work is based on the uniform representation of frequency transients in a low-inertia[1] system, as introduced in [23], [31], comprising both traditional SGs (indexed by $i\in\Omega^{\mathrm{S}}$) and CIGs (indexed by $c\in\Omega^{\mathrm{C}}$). While different generators can have slightly distinct transient frequency response, the dynamics described by the CoI swing equation with aggregate inertia M_s and damping D_s has been shown to capture accurately the system behaviour [26], [31].

In line with previous research works and industry applications, the low-order model proposed in [26] is used for modeling the governor droop and turbine dynamics. The impact of *grid-supporting* CIGs providing frequency support via droop ($d\in\Omega^{\mathrm{C}}_d\subseteq\Omega^{\mathrm{C}}$) and VSM ($v\in\Omega^{\mathrm{C}}_v\subseteq\Omega^{\mathrm{C}}$) control is also included, as these are the two most common control approaches in the literature [32], [33]. Hence, the transfer function $G(s)$ between the active power change $\Delta P_e(s)$, with positive values corresponding to a net load decrease, and the CoI frequency deviation $\Delta f(s)$ can be derived as:

$$G(s) = \frac{\Delta f(s)}{\Delta P_e(s)} = \Bigg(\underbrace{(sM_s+D_s) + \sum_{i\in\Omega^{\mathrm{S}}}\frac{K_i(1+sF_iT_i)}{R_i(1+sT_i)}}_{\text{traditional SGs}} + \underbrace{\sum_{d\in\Omega^{\mathrm{C}}_d}\frac{K_d}{R_d(1+sT_d)}}_{\text{droop-based CIGs}} + \underbrace{\sum_{v\in\Omega^{\mathrm{C}}_v}\frac{sM_v+D_v}{1+sT_v}}_{\text{VSM-based CIGs}}\Bigg)^{-1}. \tag{3}$$

It is noteworthy to mention that the droop-based CIGs consider only the damping capability of the converter (i.e., $D=1/R_d$) while the VSM-based CIGs consider both the damping and the inertia capability of the converter (i.e., D_v and M_v, respectively) [31].

Assuming that the time constants ($T_i\approx T$) of all SGs are several orders of magnitude higher than the ones of converters [34], one can approximate $T\gg T_{d,v}\approx 0$, which transforms (3) into:

$$G(s) = \frac{1}{MT}\frac{1+sT}{s^2+2\zeta\omega_n s+\omega_n^2}, \tag{4}$$

where $\omega_n = \sqrt{\frac{D+R_s}{MT}}$ and $\zeta = \frac{M+T(D+F_s)}{2\sqrt{MT(D+R_s)}}$. The definitions of the parameters in (4) and the formulation of the frequency

[1]The term "low-inertia" is primarily used to characterize the nature of the converter-dominated power system, not to apply that the damping of such system is unchanged.

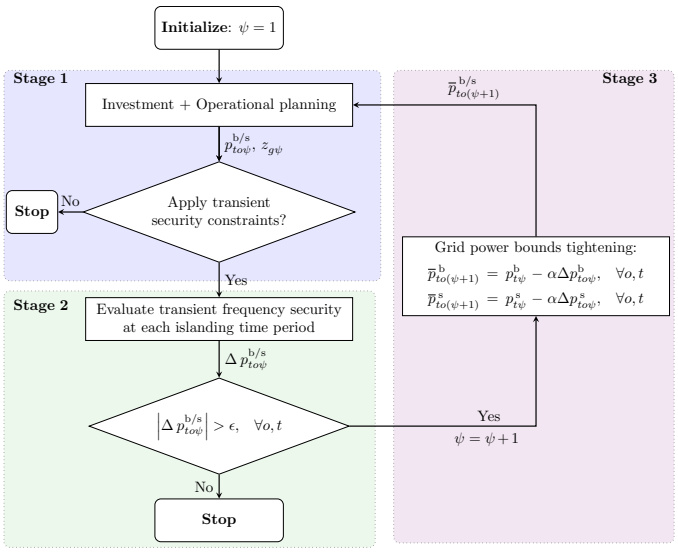

Fig. 1. Proposed three-stage MG planning algorithm.

model have been summarized in Appendix A. More details on the proposed second-order frequency model in (4) and mathematical formulation can be found in [31].

C. Dynamic Metrics for Microgrid Islanding

Following a disturbance, the dynamic frequency response is characterized by the instantaneous RoCoF ($\dot{f}_{\max}$) and frequency nadir ($\Delta f_{\max}$), whereas the steady-state response is governed by the constant frequency deviation from a pre-disturbance equilibrium ($\Delta f_{\rm ss}$). By assuming a stepwise disturbance in the active power $\Delta P_e(s) = -\Delta P/s$, where ΔP is the net power change, the time-domain expression for frequency metrics of interest can be derived as follows:

$$\dot{f}_{\max} = \dot{f}(t_0^+) = -\frac{\Delta P}{M}, \tag{5a}$$

$$\Delta f_{\max} = -\frac{\Delta P}{D + R_g}\left(1 + \sqrt{\frac{T(R_g - F_g)}{M}}e^{-\zeta\omega_n t_m}\right), \tag{5b}$$

$$\Delta f_{\rm ss} = -\frac{\Delta P}{D + R_g}, \tag{5c}$$

with the introduction of new variable $\omega_d = \omega_n\sqrt{1-\zeta^2}$ and $t_m = \left({}^{1}\!/_{\omega_d}\right)\tan^{-1}\left({}^{\omega_d}\!/_{(\omega_n\zeta - T^{-1})}\right)$ denoting the time instance of frequency nadir.

It can be clearly seen that the aggregate system parameters such as M, D, R_g and F_g have a direct impact on frequency performance. In particular, RoCoF and steady-state deviation are explicitly affected by M and (D, R_g), respectively, while frequency nadir has a non-linear dependency on all four system factors. With the increasing penetration of CIGs and subsequent decommissioning of conventional SGs, these parameters are drastically reduced and can compromise the overall frequency performance. To prevent the accidental activation of load-shedding, under/over frequency and RoCoF protection relays, the proposed three-stage solution algorithm, described in the following, imposes limits on the aforementioned frequency metrics to account for low levels of inertia and damping and their impact on the frequency response after a MG islanding.

D. Three-Stage Solution Algorithm

The proposed three-stage approach proposed for solving the problem (2) with the inclusion of static and transient security constraints is illustrated in Fig. 1 and can be summarized as follows:

1) Solving the Static Investment Planning Problem: At each iteration ψ, the investment planning model (2) is solved under static security constraints in both grid-connected and islanded mode. In the case that transient frequency security is desired to ensure MG survivability during abrupt islanding, the process flow to Stages 2 and 3 can be adopted. Otherwise, the process flow terminates at Stage 1 where only grid-connected and static islanding requirements are met. A detailed formulation is provided in Section III-A.

2) Evaluating Transient Frequency Security: The unscheduled loss of power exchange with the main grid may result in large frequency transients within the MG. Following the discussion from Section II-C, the transient frequency response is characterized by the magnitude of the abrupt active power loss (ΔP) and the aggregate control parameters of all MG generators (M, D, R_g, and F_g). Therefore, the magnitude of the potential disturbance at each hour of every representative day during the planning horizon is set equal to the power exchange with the main grid scheduled at the time of the disconnection (i.e., $\Delta P = p^{\rm b/s}_{to\psi}$). At the same time, the control parameters depend on the built/not-built status of generators in the MG at each iteration ($z_{g\psi}$). Consequently, at each iteration ψ, this stage of the algorithm uses the variables $p^{\rm b/s}_{to\psi}$ and $z_{g\psi}$ obtained from the first stage to evaluate the solution feasibility under transient security constraints in (5), described in detail in Section III-B.

The solution of the second stage provides the minimum amount of corrective deviation ($\Delta p^{\rm b/s}_{to\psi}$) from the scheduled power exchange with the main grid ($p^{\rm b/s}_{to\psi}$) to meet the transient security criteria. If this value is zero or less than a small tolerance (ϵ), the optimal investment and operational solution obtained from the first-stage problem ensures frequency security in islanded mode, and the algorithm is terminated. Otherwise, the algorithm proceeds to the third stage.

3) Tightening Power Exchange with the Main Grid: The third stage of the algorithm employs the non-zero solution obtained from the previous stage to tighten the limits imposed on the power exchange with the main grid at each hour of every representative day throughout the planning horizon. Once the bounds have been altered, the algorithm proceeds to the next iteration ($\psi+1$). The modified limits may lead either to a change in the power exchange with the main grid (through operational decisions), a change in the investment decisions, or both.

III. Extended Formulation under Static and Transient Constraints

In this section, the extended formulation of the proposed planning tool under static and transient constraints is presented. The iteration index ψ is omitted for better legibility and brevity.

A. Extended Formulation under Static Constraints

The optimization problem in the first stage corresponds to the compact formulation (2), including investment limitations and static operational constraints in grid-connected and islanded mode. The extended terms in the objective function and the constraints are outlined in the following.

1) Investment: The term $\Theta^{\mathrm{inv}}(\chi^{\mathrm{inv}})$ in the objective function of the proposed planning problem is given by:

$$\min_{\chi^{\mathrm{inv}}} \ \Theta^{\mathrm{inv}} = \sum_{g\in\{\Omega^{\mathrm{S}},\Omega^{\mathrm{C}}\}} (ic_g \cdot z_g) + \sum_{(n,n')\in\Omega^{\mathrm{L}}} (ic_{nn'} \cdot z_{nn'}), \quad (6)$$

and includes the total investment/reinforcement costs of generators/lines throughout the planning horizon. The optimization variables $\chi^{\mathrm{inv}} = \{z_g, z_{nn'}\}, \forall g \in \{\Omega^{\mathrm{S}}, \Omega^{\mathrm{C}}\} \wedge \forall (n,n') \in \Omega^{\mathrm{L}}$ are *here-and-now* decisions (i.e. not a function of uncertain parameters, and thus, non-adjustable) [35].

2) Grid-Connected Operation: The function $\Theta^{\mathrm{gm,opr}}$ capturing the operational cost in grid-connected mode is given by:

$$\begin{aligned}\min_{\chi^{\mathrm{gm,opr}}} \ \Theta^{\mathrm{gm,opr}} = &\sum_{o\in\Omega^{\mathrm{O}}}\sum_{t\in\Omega^{\mathrm{T}}} \left(\tau_o \cdot \left(e^{\mathrm{b}}_{to} \cdot p^{\mathrm{b}}_{to} - e^{\mathrm{s}}_{to} \cdot p^{\mathrm{s}}_{to}\right)\right) \\ &+ \sum_{o\in\Omega^{\mathrm{O}}}\sum_{t\in\Omega^{\mathrm{T}}}\sum_{g\in\{\Omega^{\mathrm{S}},\Omega^{\mathrm{C}}\}} (\tau_o \cdot mc_g \cdot p_{gto}) \\ &+ \sum_{o\in\Omega^{\mathrm{O}}}\sum_{t\in\Omega^{\mathrm{T}}}\sum_{n\in\Omega^{N}} \left(\tau_o \cdot fc_n \cdot d^{\mathrm{p}f}_{nto}\right)\end{aligned} \quad (7a)$$

The constraints that need to be taken into account to reflect operational limitations in grid-connected mode are:

Constraints on active and reactive power flows:

$$\begin{aligned} &p_{n''nto} + p^{\mathrm{b}}_{to|n=1} - p^{\mathrm{s}}_{to|n=1} + \sum_{g\in\{\Omega^{\mathrm{Sn}},\Omega^{\mathrm{Cn}}\}} p_{gto} \\ &\quad = \sum_{n'\in\Omega^{\mathrm{Nn}}} p_{nn'to} + d^{\mathrm{p}}_{nto}, \qquad \forall n,t,o, \end{aligned} \quad (7b)$$

$$\begin{aligned} &q_{n''nto} + q^{\mathrm{b}}_{to|n=1} - q^{\mathrm{s}}_{to|n=1} + \sum_{g\in\{\Omega^{\mathrm{Sn}},\Omega^{\mathrm{Cn}}\}} q_{gto} \\ &\quad = \sum_{n'\in\Omega^{\mathrm{Nn}}} q_{nn'to} + d^{\mathrm{q}}_{nto}, \qquad \forall n,t,o, \end{aligned} \quad (7c)$$

$$v_{n''to} - v_{nto} = \left(r_{n''n} \cdot p_{n''nto} + x_{n''n} \cdot q_{n''nto}\right), \ \forall n,t,o, \quad (7d)$$

Constraints on power exchange with the main grid:

$$0 \le p^{\mathrm{b}}_{to} \le \overline{p}^{\mathrm{b}}_{to}, \ 0 \le p^{\mathrm{s}}_{to} \le \overline{p}^{\mathrm{s}}_{to}, \qquad \forall t,o, \quad (7e)$$

$$0 \le q^{\mathrm{b}}_{to} \le \overline{q}^{\mathrm{b}}_{to}, \ 0 \le q^{\mathrm{s}}_{to} \le \overline{q}^{\mathrm{s}}_{to}, \qquad \forall t,o, \quad (7f)$$

Constraints on constant and flexible load:

$$d^{\mathrm{p}}_{nto} = d^{\mathrm{pc}}_{nto} + d^{\mathrm{pf}}_{nto}, \qquad \forall n,t,o, \quad (7g)$$

$$d^{\mathrm{q}}_{nto} = d^{\mathrm{qc}}_{nto} + d^{\mathrm{qf}}_{nto}, \qquad \forall n,t,o, \quad (7h)$$

$$\underline{d}^{\mathrm{pf}}_{nto} \le d^{\mathrm{pf}}_{nto} \le \overline{d}^{\mathrm{pf}}_{nto}, \qquad \forall n,t,o, \quad (7i)$$

$$\underline{d}^{\mathrm{qf}}_{nto} \le d^{\mathrm{qf}}_{nto} \le \overline{d}^{\mathrm{qf}}_{nto}, \qquad \forall n,t,o, \quad (7j)$$

$$\sum_{t\in\Omega^{T}} d^{\mathrm{p}}_{nto} = e_{no}, \qquad \forall n,o, \quad (7k)$$

Constraints on power generation of different units:

$$0 \le p_{gto} \le \overline{p}_{gto} \cdot z_g, \qquad \forall g \in \{\Omega^{\mathrm{S}},\Omega^{\mathrm{C}}\}, t, o, \quad (7l)$$

$$\overline{p}_{gto} = p^{\mathrm{nom}}_g - p^{\mathrm{FR}}_g, \qquad \forall g \in \{\Omega^{\mathrm{S}}\}, t, o, \quad (7m)$$

$$\overline{p}_{gto} = \min(p^{\mathrm{nom}}_g - p^{\mathrm{FR}}_g, p^{\mathrm{AV}}_{gto}), \qquad \forall g \in \{\Omega^{\mathrm{C}}\}, t, o, \quad (7n)$$

$$\underline{q}_{gto} \cdot z_g \le q_{gto} \le \overline{q}_{gto} \cdot z_g, \qquad \forall g \in \{\Omega^{\mathrm{C}},\Omega^{\mathrm{S}}\}, t, o, \quad (7o)$$

$$-r^{\mathrm{d}}_g \le p_{gto} - p_{g(t-1)o} \le r^{\mathrm{u}}_g, \qquad \forall g \in \Omega^{\mathrm{S}}, t, o, \quad (7p)$$

$$\sum_{t\in\Omega^{T}} p_{gto} + e^{\mathrm{FR}}_g \le c_{go} \cdot \sum_{t\in\Omega^{T}} \overline{p}_{gto}, \qquad \forall g \in \Omega^{\mathrm{S}}, o, \quad (7q)$$

Constraints on line thermal limits:

$$p^2_{nn'to} + q^2_{nn'to} \le \overline{s}^2_{nn'} \cdot \left(z^0_{nn'} + z_{nn'}\right), \qquad \forall (n,n') \in \Omega^{\mathrm{L}}, o, \quad (7r)$$

Constraints on nodal voltage magnitudes:

$$\underline{v} \le v_{nto} \le \overline{v}, \ v_{to|n=1} = 1, \qquad \forall n,t,o, \quad (7s)$$

Here, the vector of *wait-and-see* decision variables (i.e. a function of uncertain parameters, and thus, adjustable) [35] is given by $\chi^{\mathrm{gm,opr}} = \{d^{\mathrm{p/q}}_{nto}, d^{\mathrm{pf/qf}}_{nto}, p_{gto}, p_{nn'to}, p^{\mathrm{b/s}}_{to}, q_{gto}, q_{nn'to}, q^{\mathrm{b/s}}_{to}, v_{nto}\}$.

The objective function (7a) minimizes the total operation costs, including the total costs of power exchange with the main grid, the total operation costs of generators, and the total penalty costs of shifting loads away from the periods preferred by consumers. Constraints (7b)-(7d) describe the power flows based on the linearized version of the DistFlow model [28], [29], and (7e)-(7f) ensure the non-negativity and impose the upper limits on the power exchange with the main grid. Note that $p^{\mathrm{b/s}}_{to}$ and $q^{\mathrm{b/s}}_{to}$ in (7b) and (7c) are included only at the Point-of-Common Coupling (PCC) node denoted by $n = 1$. Furthermore, (7g)-(7j) reflect the power balance of constant and flexible loads as well as the limitations of flexible loads at each node and at every hour of each representative day, whereas (7k) ensures that the daily energy consumption of flexible loads is maintained for each representative day. Constraints (7l)-(7p) denote capacity, reserve and ramp-rate limits of generators at each hour of every representative day. Parameter p^{FR}_g in (7l) and (7n) relates to the minimum active power reserve capacity of each generator allocated to transient frequency control. This requirement can be predefined by the grid code [36] or calculated as $p^{\mathrm{FR}}_g = \left(M_g \dot{f}_{\mathrm{lim}} + (D_g + R_g)\Delta f_{\mathrm{lim}}\right)$ with $\dot{f}_{\mathrm{lim}}$, and Δf_{lim} denoting the maximum acceptable RoCoF, and frequency deviation prior to under-frequency load shedding, respectively. The energy adequacy for transient performance, defined by parameter e^{FR}_g, is calculated as $e^{\mathrm{FR}}_g = \left(M_g \dot{f}_{\mathrm{lim}} T^{\mathrm{FC^I}} + (D_g + R_g)\Delta f_{\mathrm{lim}} T^{\mathrm{FC^P}}\right)$ where $T^{\mathrm{FC^I}}$ and $T^{\mathrm{FC^P}}$ define the delivery periods for inertia and primary frequency response, respectively. It should be noted here that delivery periods $T^{\mathrm{FC^I}}$ and $T^{\mathrm{FC^P}}$ include all hours considered in the planning horizon of each representative day. Energy reserves (e^{FR}_g) for transient frequency control in CIGs is commonly provided by three different approaches, i.e. can be provided by the converter-side DC-link capacitor energy storage [37], by a battery energy storage attached to the CIG [38], or by decreasing the CIG output from the maximum power point to allow for upward regulation. In this paper, we assume that the energy and power reserves for transient frequency control of CIG units are provided by the DC-side capacitor as detailed in [37]. Furthermore, (7l)-(7n) limit the SG and CIG output power to accommodate for the necessary power reserves (p^{FR}_g). For the synchronous units the maximum available power $\overline{p}_{gto}$ is given by the unit's power capacity reduced in order to account for the frequency reserves required (7m). On the other hand, for CIG units the power output at any time period is dependent on the weather conditions and as such its maximum power point at each hour p^{AV}_g will further limit the available power that can be dispatched (7n). Moreover, the reactive power limits of CIGs are based on the maximum generated active power, i.e.,

$\overline{q}_{gto} = \tan\phi \cdot \overline{p}_{gto}$, where $\cos\phi$ is the maximum power factor of a unit defined by the grid code. Constraint (7q) defines the daily capacity factor of SGs in each representative day of the planning horizon [39], and (7r) imposes the thermal loading limits of each line. The latter quadratic constraint is linearized by means of a convex polygon, defined by inner approximations of the thermal loading circle [30]. Finally, (7s) limits the nodal voltage magnitudes throughout the planning horizon.

3) Islanded Operation: It is assumed that at every hour of each representative day, the MG should be able to withstand an unscheduled islanding event. The operation planning problem of a MG in islanded mode is aimed at ensuring survivability and self-sufficiency, where priority is given to critical loads. It is worthwhile to note that, in this paper, the self-sufficiency is ensured for one period (i.e., one hour) after disconnection from the main grid. However, the islanded operation period can be straightforwardly extended to multiple periods based on the required resilience. Hereafter, the superscript "im" denotes operational variables in islanded mode. The function $\Theta_{to}^{\mathrm{im,opr}}$ capturing the operational cost in islanded mode is given by:

$$\min_{\chi_{to}^{\mathrm{im,opr}}} \quad \Theta_{to}^{\mathrm{im,opr}} = \sum_{n\in\Omega^{\mathrm{N}}} \left(pc_n \left((1-y_{nto})\, d_{nto}^{\mathrm{p_c}} + \hat{d}_{nto}^{\mathrm{p_f^-}} \right) \right) \tag{8a}$$

The constraints that need to be taken into account to reflect operational limitations in islanded mode are:

Constraints on the active and reactive power flows:

$$p_{n''nto}^{\mathrm{im}} + \sum_{g\in\{\Omega^{\mathrm{S_n}},\Omega^{\mathrm{C_n}}\}} p_{gto}^{\mathrm{im}} = \sum_{n'\in\Omega^{\mathrm{N_n}}} p_{nn'to}^{\mathrm{im}} + \left(y_{nto}\cdot d_{nto}^{\mathrm{p_c}} + d_{nto}^{\mathrm{im,p_f}} \right), \quad \forall n,t,o, \tag{8b}$$

$$q_{n''nto}^{\mathrm{im}} + \sum_{g\in\{\Omega^{\mathrm{S_n}},\Omega^{\mathrm{C_n}}\}} q_{gto}^{\mathrm{im}} = \sum_{n'\in\Omega^{\mathrm{N_n}}} q_{nn'to}^{\mathrm{im}} + \left(y_{nto}\cdot d_{nto}^{\mathrm{q_c}} + d_{nto}^{\mathrm{im,q_f}} \right), \quad \forall n,t,o, \tag{8c}$$

$$v_{n''to}^{\mathrm{im}} - v_{nto}^{\mathrm{im}} = \left(r_{n''n}\cdot p_{n''nto}^{\mathrm{im}} + x_{n''n}\cdot q_{n''nto}^{\mathrm{im}} \right), \quad \forall n,t,o, \tag{8d}$$

Constraints on the constant and flexible load:

$$d_{nto}^{\mathrm{im,p_f}} = d_{nto}^{\mathrm{p_f}} + \hat{d}_{nto}^{\mathrm{p_f^+}} - \hat{d}_{nto}^{\mathrm{p_f^-}}, \quad \forall n,t,o, \tag{8e}$$

$$d_{nto}^{\mathrm{im,q_f}} = d_{nto}^{\mathrm{q_f}} + \hat{d}_{nto}^{\mathrm{q_f^+}} - \hat{d}_{nto}^{\mathrm{q_f^-}}, \quad \forall n,t,o, \tag{8f}$$

$$0 \le \hat{d}_{nto}^{\mathrm{p_f^+}}, \hat{d}_{nto}^{\mathrm{q_f^+}}, \hat{d}_{nto}^{\mathrm{p_f^-}}, \hat{d}_{nto}^{\mathrm{q_f^-}}, \quad \forall n,t,o, \tag{8g}$$

$$\underline{d}_{nto}^{\mathrm{p_f}} \le d_{nto}^{\mathrm{im,p_f}} \le \overline{d}_{nto}^{\mathrm{p_f}}, \quad \forall n,t,o, \tag{8h}$$

$$\underline{d}_{nto}^{\mathrm{q_f}} \le d_{nto}^{\mathrm{im,q_f}} \le \overline{d}_{nto}^{\mathrm{q_f}}, \quad \forall n,t,o, \tag{8i}$$

$$d_{nto}^{\mathrm{im,p}} \le e_{no} - \sum_{t'=1}^{t-1} d_{nt'o}^{\mathrm{p}}, \quad \forall n,t,o, \tag{8j}$$

Constraints on power generation of different units:

$$0 \le p_{gto}^{\mathrm{im}} \le \overline{p}_{gto}\cdot z_g, \quad \forall g\in\{\Omega^{\mathrm{C}},\Omega^{\mathrm{S}}\},t,o, \tag{8k}$$

$$\underline{q}_{gto}\cdot z_g \le q_{gto}^{\mathrm{im}} \le \overline{q}_{gto}\cdot z_g, \quad \forall g\in\{\Omega^{\mathrm{C}},\Omega^{\mathrm{S}}\},t,o, \tag{8l}$$

$$-r_g^{\mathrm{d}} \le p_{gto}^{\mathrm{im}} - p_{gto} \le r_g^{\mathrm{u}}, \quad \forall g\in\Omega^{\mathrm{S}},t,o, \tag{8m}$$

$$p_{gto}^{\mathrm{im}} \le c_{go}\cdot \sum_{t\in\Omega^T} \overline{p}_{gto} - \sum_{t'=1}^{t-1} p_{gto}, \quad \forall g\in\Omega^{\mathrm{S}},t,o, \tag{8n}$$

Constraints on line thermal limits:

$$p_{nn'to}^{\mathrm{im}\ 2} + q_{nn'to}^{\mathrm{im}\ 2} \le s_{nn'to}^2 \cdot \left(z_{nn'}^0 + z_{nn'} \right), \quad \forall (n,n')\in\Omega^{\mathrm{L}},t,o, \tag{8o}$$

Constraints on nodal voltage magnitudes:

$$\underline{v} \le v_{nto}^{\mathrm{im}} \le \overline{v},\ v_{to|n=1}^{\mathrm{im}} = 1, \quad \forall n,t,o, \tag{8p}$$

where, similarly to the previous operation planning problem in grid-connected mode, all operation variables $\chi_{to}^{\mathrm{im,opr}} = \{\hat{d}_{nto}^{\mathrm{p_f/q_f}}, d_{nto}^{\mathrm{im,p_f/im,q_f}}, \hat{p}_{gto}, p_{gto}^{\mathrm{im}}, p_{nn'to}^{\mathrm{im}}, \hat{q}_{gto}, q_{gto}^{\mathrm{im}}, q_{nn'to}^{\mathrm{im}}, v_{nto}^{\mathrm{im}}\}$ are *wait-and-see* decisions.

The objective function (8a) minimizes the total unserved load and ensures an adequate supply of at least the critical MG loads. It should be noted that pc_n describes the priority level of the load at a specific node, with higher values suggesting more critical loads, and the amount of unserved flexible load is denoted by $\hat{d}_{nto}^{\mathrm{p_f}}$. Constraints (8b)-(8d) enforce the post-islanding power flow balance, whereas the deviations between the amount of flexible load served in grid-connected and islanded mode are given by (8e)-(8f) and used to determine the fraction of served and unserved flexible loads in islanded mode. Moreover, (8h)-(8i) enforce the limitations of flexible loads in islanded mode, and (8j) restricts the supply of flexible loads in terms of respective demand already served before the current time instance affected by a disconnection from the main grid. Constraints (8k)-(8l) denote capacity limits of generators, (8m)-(8n) indicate that re-scheduling actions of SGs in islanded mode are subject to their ramp rate and daily capacity factor limitations as well as their scheduling actions before the current time step. Furthermore, similar to the formulation in grid-connected mode, (8o) defines the thermal loading limit of each line and (8p) limit the nodal voltage magnitudes. In the grid-connected mode the voltage at the PCC is maintained by the stiff grid, while in the islanded mode it is controlled by the DERs.

The final optimization problem is a MILP problem in the first stage of the algorithm, and its solution is subsequently used in the feasibility check in the second stage.

B. Formulation of the Transient Security Problem

The feasibility of the planning solution under transient security constraints is necessary to guarantee the secure islanding of a MG. According to the metrics described in (5) and the discussions in Section II-D, the transient frequency response in the event of islanding depends on the amount of power exchange with the main grid at the time of the event (i.e., $\Delta P = p_{to\psi}^{\mathrm{b/s}}$) and the control parameters of the online generators in the MG (i.e., $M(z_{g\psi})$, $D(z_{g\psi})$, $F_g(z_{g\psi})$ and $R_g(z_{g\psi})$). Note however that, with respect to decision variables, (5a) and (5c) are linear while (5b) is highly non-linear. Given the optimal values of decision variables obtained from the first stage ($p_{to\psi}^{\mathrm{b/s}}$ and $z_{g\psi}$), the non-linear term in (5b) can be defined as a constant at each iteration. Consequently, at each iteration ψ, the feasibility check can be formulated as a linear programming problem of the form

$$\Theta_t^{\mathrm{dyn}} = \min_{\Delta p_{to\psi}^{\mathrm{b/s}}} \left| \Delta p_{to\psi}^{\mathrm{b/s}} \right| \tag{9a}$$

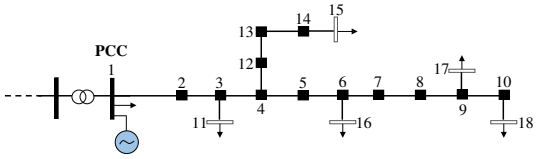

Fig. 2. Modified CIGRE European low voltage network.

The constraints that need to be taken into account to ensure transient security feasibility are:

$$\left|\frac{p^{\mathrm{b/s}}_{to\psi}+\Delta p^{\mathrm{b/s}}_{to\psi}}{M}\right| \leq \dot{f}_{\mathrm{lim}}, \tag{9b}$$

$$\left|\frac{p^{\mathrm{b/s}}_{to\psi}+\Delta p^{\mathrm{b/s}}_{to\psi}}{D+R_g}\cdot\left(1+\sqrt{\frac{T(R_g-F_g)}{M}}e^{-\zeta\omega_n t_m}\right)\right| \leq \Delta f_{\mathrm{lim}}, \tag{9c}$$

$$\left|\frac{p^{\mathrm{b/s}}_{to\psi}+\Delta p^{\mathrm{b/s}}_{to\psi}}{D+R_g}\right| \leq \Delta f_{\mathrm{ss,lim}}. \tag{9d}$$

The feasibility checking problem (9) is solved independently for each hour t of every representative day o. Constraints (9b)-(9d) enforce permissible frequency response limits pertaining to RoCoF, frequency nadir, and quasi-steady-state frequency deviation [36], respectively, whereas slack variables $\Delta p^{\mathrm{b/s}}_{to\psi}$ are used to identify the violations of transient security limits at a specific hour and iteration. Accordingly, (9a) provides the minimum change needed in the scheduled power exchange with the main grid from the first stage to ensure frequency security. After solving (9) for each considered time step at each iteration ψ, the value of $\Delta p^{\mathrm{b/s}}_{to\psi}$ is used to modify and tighten the power exchange limits with the main grid at the next iteration $(\psi+1)$:

$$\overline{p}^{\,\mathrm{b}}_{to(\psi+1)} = p^{\mathrm{b}}_{to\psi} - \alpha\Delta p^{\mathrm{b}}_{to\psi}, \qquad \forall t,o, \tag{10a}$$

$$\overline{p}^{\,\mathrm{s}}_{to(\psi+1)} = p^{\mathrm{s}}_{to\psi} - \alpha\Delta p^{\mathrm{s}}_{to\psi}, \qquad \forall t,o. \tag{10b}$$

The scaling factor α is used to apply a less conservative bound modification to account for intertemporal power shifting and investment candidates with frequency support. Furthermore, α prevents the emergence of oscillatory non-convergence that might occur due to the multi-stage nature of the solution algorithm. In this work, a value of $\alpha \in [0.5, 0.7]$ was adopted, calculated through a heuristic approach. Alternatively, a line-search approach could be implemented in the algorithm, allowing to select the maximum α that satisfies the requirements while minimizing the computational time.

The proposed algorithm (see Fig. 1) can be summarized as:

Stage 1: Investment and operational planning with static security, (6)-(8);
Stage 2: Transient security evaluation at all hours, (9);
Stage 3: Grid power bounds tightening, (10).

IV. Case Study

A. System Description

A modified CIGRE residential low-voltage network [40], illustrated in Fig. 2, is used to analyze the performance of the proposed planning tool. It is assumed that one SG is already preset at PCC (SG_1) and the investment candidates comprise one SG (SG_2) and three PV CIGs (i.e., PV_1 and PV_2 interfaced via *grid-supporting* converters, and PV_3 operating in *grid-feeding* mode with fixed power output). The fundamental control parameters obtained from [23] and investment costs (derived from [12], [41]) of all generators are provided in Table I, while system operation costs are given in Table II. Note that the fixed operational costs are included as a markup in the annualised investment costs while the variable operational costs are as defined in Table II. The load parameters are defined in Table III where $50\,\%$ of nominal load connected at node 1 is shiftable, whereas high priority critical loads are connected at nodes 15 and 16. The patterns of loads and PV generation in Texas during 2016 [42] are used to obtain representative days through k-means clustering. Note that all representative days for loads and PV generations are provided in Appendix B. The transient security constraints are enforced through thresholds imposed on RoCoF ($\dot{f}_{\mathrm{lim}} = 2\,\mathrm{Hz/s}$), frequency nadir ($\Delta f_{\mathrm{lim}} = 0.8\,\mathrm{Hz}$), and quasi-steady-state frequency deviation ($\Delta f_{\mathrm{ss,lim}} = 0.2\,\mathrm{Hz}$). Also, a value of $\epsilon = 10^{-2}$ is adopted. The implementation was done in MATLAB, with the optimization model formulated in YALMIP [43] and solved by Gurobi [44].

TABLE I
Generator Control Parameters and Investment Costs

	SG_1	SG_2	PV_1	PV_2	PV_3
Annualized investment cost ($)	-	40 000	70 000	65 000	60 000
Capacity (kW)	280	350	350	350	350
Node	1	15	17	11	18
M (s)	14	14	14	-	-
D (p.u.)	25	25	30	-	-
K (p.u.)	1	1	1	1	-
R (p.u.)	0.03	0.03	-	0.05	-
F (p.u.)	0.35	0.35	-	-	-
Existing generator					
Candidate generators					

TABLE II
System Operation Costs

Import ($/kWh)	Export ($/kWh)	SG ($/kWh)	PV ($/kWh)	Demand shift penalty ($/kWh)	Demand disconnection penalty ($/kWh)
30	15	60	0	100	$(150-200)^*$

*Based on the level of demand criticality, only in islanded mode

To analyze the performance of the proposed planning tool, three cases are considered:

Case 1: MG planning without robust islanding constraints (stochastic approach);
Case 2: MG planning with only robust static islanding constraints (stochastic-robust approach);
Case 3: MG planning with robust static and transient frequency islanding constraints (stochastic-robust approach).

Cases 1 and 2 consider only Stage 1, while Case 3 considers all the stages of the proposed algorithm.

B. Cost Analysis

In this analysis, the costs of the three aforementioned case studies are compared under the consideration of four representative days. Let us first study Case 1, with the respective costs under different capacity limits of the main feeder listed in Table IV. For conciseness, we will present the result obtained with

TABLE III
LOAD PARAMETERS (F: FLEXIBLE, C: CONSTANT)

Node	1	11	15	16	17	18
Type	F	C	C	C	C	C
Nominal Load [kVA]	200	15	52	210	35	47
Power factor	0.95	0.95	0.95	0.85	0.95	0.95

High priority load
Low priority load

TABLE IV
COST COMPARISON WITH VARIATION IN MAIN GRID CAPACITY FOR CASE 1: MG PLANNING WITHOUT ISLANDING CONSTRAINTS

Main grid capacity (kW)	Investment costs & decisions ($)	Operational costs ($)	Total costs ($)	Installed capacity (kW)
Unlimited	0	56 394	56 394	280
250	0	77 795	77 795	280
150	60 000 (PV_3)	47 473	107 473	630

four representative days and scenarios illustrated by the profiles in Appendix A (Fig. 9). Understandably, the MG mainly relies on more affordable power provided by the main grid instead of dispatching SG_1 installed at PCC. Under the unlimited import capacity from the main grid, investments in local generation are not economical due to the low cost of imported power. However, with the introduction of grid capacity limits (e.g., in instances of net load growth and faults experienced in the network), the operational costs increase as a result of the MG relying on the more expensive SG_1 at PCC. Further reduction of grid capacity finally leads to the installment of PV_3, as it yields higher investment but lower operational costs compared to SG_2 and thus significantly reduces the overall operational costs.

The variation between investment and operational costs for Cases 2 and 3 is provided in Table V, where the optimal solution at iteration $\psi = 1$ corresponds to the optimal costs of Case 2. Note that the problem in Cases 2 and 3 is solved considering unlimited power import from the main grid. The MG requires higher reliability in Case 2 compared to Case 1 in order to minimize the loss of load under static security constraints, whereas in Case 3 the survivability and resilience of the MG are also considered by including the transient security constraints. To ensure the MG resilience, higher investment and operational costs are enforced in both of these case studies compared to Case 1 due to inclusion of static and transient islanding constraints. Indeed, a $400\,\%$ cost increase for Case 2 is observed, with a further $10\,\%$ increase for Case 3. In both of these cases, the installation of renewable DERs reduces the total costs despite the significantly higher underlying investment costs. More precisely, renewable DERs contribute to increased line flows and power export to the main grid, thus necessitating a greater network capacity indicated by the upgrade of the lines between nodes (1-2) and (2-3). However, in turn, the MG adequacy improves with installing renewable DERs, reflected in the reduction of lost load and ensuring that critical loads are supplied even during emergency islanding situations.

Focusing on Case 3, it is noticeable that operational costs increase at each iteration due to the use of expensive SGs and flexible loads to mitigate the feasibility violation. Nevertheless, when operational flexibility alone cannot guarantee security, more units are installed. Finally, it can be seen that tightening of

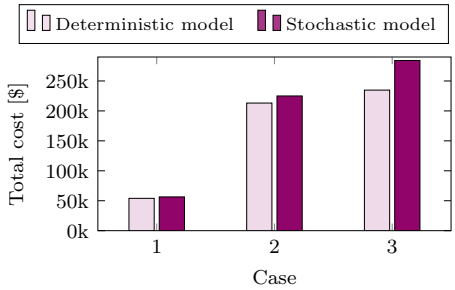

Fig. 3. Total costs for deterministic and stochastic models in Cases 1, 2 and 3.

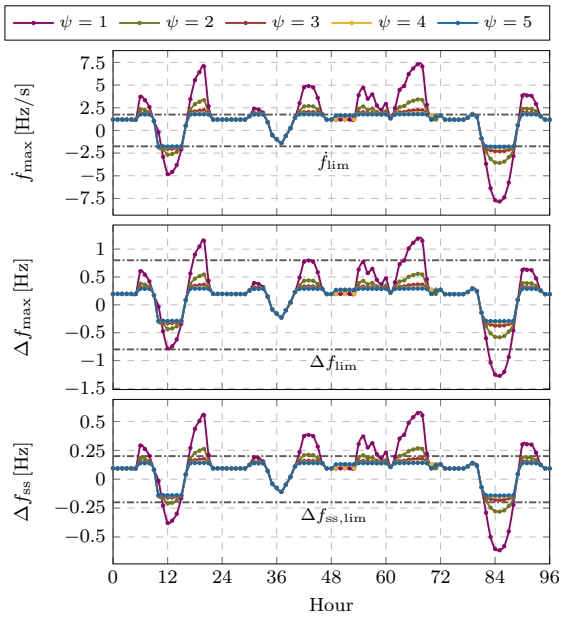

Fig. 4. System performance in terms of the transient frequency metrics for different iterations of the proposed algorithm including four representative days.

the power exchange limits (and thus the power export) with the main grid alleviates some of the necessary network investments (e.g., line (3-11) for iterations 1 and 2). Thus, the MG planner can be made aware of the enforced additional cost to ensure the resilience of the system through including transient security constraints in Case 3 as compared to Case 2.

In Fig. 3, a comparison of the total design costs considering either a deterministic/stochastic (Case 1) or deterministic/stochastic-robust (Case 2 & 3) model in all three cases is presented. Note that the deterministic model in Cases 1, 2, and 3 considers only one representative day (i.e., the average daily load and power generation patterns). As noticeable in Fig. 3, a deterministic model provides a rather optimistic solution that can lead to system vulnerabilities for both static and transient security. This risk is shown to grow with the inclusion of transient security (Case 3). Hence, increasing the number of scenarios provides a more accurate system representation, which ensures a more robust design. This is further analyzed in Section IV-D1.

C. Transient Security Analysis

In Case 3, the MG survivability is ensured by meeting the prescribed transient security criteria. In the second stage of the algorithm (see Fig. 1), the slack variable $\Delta p_{to}^{\mathrm{b/s}}$ is used to indicate the amount of adjustment needed in the scheduled

TABLE V
PLANNING COSTS FOR CASE 2 (FINAL COST IN BLUE) AND CASE 3 (FINAL COST IN GREEN) AND AGGREGATED CORRECTIVE POWER DEVIATIONS INCLUDING FOUR REPRESENTATIVE DAYS.

ψ	Investment costs & decisions ($)	Operational costs ($)	Demand shift penalty ($)	Demand disconnection penalty ($)	Total costs ($)	Import power deviation (kW)	Export power deviation (kW)
1	128 000 (PV_2, PV_3 + Lines 1-2, 2-3, 3-11)	96 956	3 613	5 548	224 956	2 902	1 431
2	127 000 (PV_2, PV_3 + Lines 1-2, 2-3)	113 872	8 543	5 337	240 872	871	429
3	127 000 (PV_2, PV_3 + Lines 1-2, 2-3)	118 924	8 796	5 081	245 924	261	129
4	127 000 (PV_2, PV_3 + Lines 1-2, 2-3)	120 423	8 572	5 334	247 423	78	39
5	127 000 (PV_2, PV_3 + Lines 1-2, 2-3)	120 890	8 805	5 081	247 890	23	12

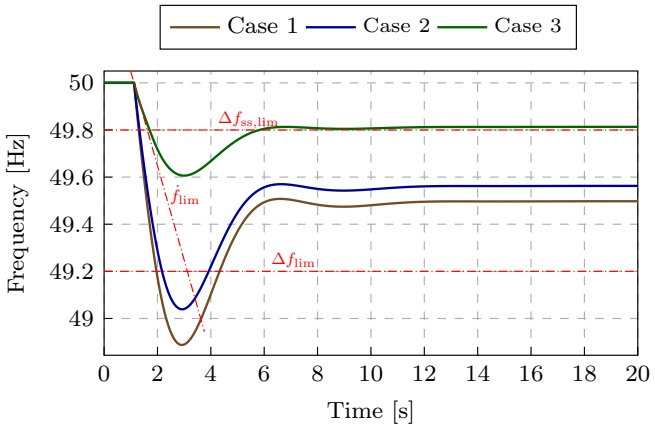

Fig. 5. MG CoI frequency response after an abrupt islanding event at hour = 20 for each of the three cases studied.

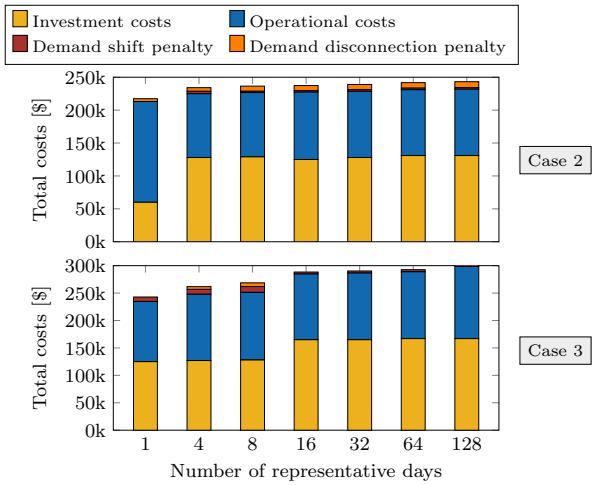

Fig. 6. Total costs for different representative days in Cases 2 and 3.

power exchange with the main grid to satisfy the transient frequency requirements. Fig. 4 showcases the metrics describing the dynamic performance of the MG's CoI after islanding at each hour. The first iteration corresponds to the system response without transient security requirements (Case 2).

A significant improvement is recorded in the maximum RoCoF values, even within a single iteration (e.g., reduction from $8\,\mathrm{Hz/s}$ to $3.5\,\mathrm{Hz/s}$ after the first iteration). Furthermore, each successive iteration reduces the power exchange with the main grid during the hours when security limits are violated until all limits are satisfied. The amount of aggregated corrective power deviations ($\sum_{o\in\Omega^O}\sum_{t\in\Omega^T}\Delta p_{to}^{\mathrm{b/s}}$) in Table V is monotonically decreased with each iteration until the transient security constraints are fulfilled. However, these improvements in terms of security and resilience are achieved at the expense of higher operational costs by dispatching costly SG and flexible loads.

It is clear from Fig. 4 that the RoCoF threshold is the most limiting factor for secure transient operation. This is expected, since PV-based CIGs yield a more economic solution but do not provide the same level of inertia as SGs, thus degrading the transient performance. In particular, SG_1 and PV_1 provide both inertia and damping, PV_2 improves damping through droop control, and PV_3 offers no frequency support. Since the inertia and damping contribution of SG_1 and PV_2 do not lead to sufficient transient performance, the reduction in the power exchange with the main grid is needed to ensure a satisfactory response. This is achieved through power provision from PV_2 and PV_3 as well as higher activation of flexible loads.

The analytical result in Fig. 4 is validated through a time-domain simulation of the MG. In the time-domain simulation, the CIGs are modeled as detailed in [34] while the SGs are modeled by a 6^{th}-order model equipped with a reheat turbine speed governor [45] and an IEEE ACIA exciter [46]. The dynamic simulations were performed with PyRAMSES [47] software. The disconnection from the grid occurs at time $= 1$ s. As indicated in Fig. 5, neither Case 1 nor Case 2 ensures a secure transition to islanded state given an abrupt islanding event. However, the solution of Case 3 ensures the transient security, and thus, survivability of the MG during the transition to the islanded mode, as shown in Fig. 5.

D. Sensitivity Analysis

1) Representative Days: The stochasticity of both load and generation profiles affects the planning accuracy, usually resulting in under- or overestimation. As previously described in Section IV-A, the load and generation profiles are obtained by utilizing the k-means clustering for different representative days. Understandably, the number of considered representative days has a direct impact on the solution of the algorithm. This can be observed in Fig. 6, where the total investment and operational costs for Cases 2 and 3 increase with the number of representative days. In particular, employing more representative days provides a better representation of system operation, thus allowing for more accurate estimates of different costs. Additionally, an increase in the representative days results in a more robust design as more scenarios for an abrupt islanding event can be taken into account during system design. On the other hand, it also imposes a higher computational burden as this results in a significant increase in the solution space of the problem

TABLE VI
INVESTMENT COSTS AND DECISIONS CONSIDERING CASES 2 AND 3 FOR DIFFERENT REPRESENTATIVE DAYS

Investment costs ($) and decisions		
Representative days	Case 2	Case 3
1	60000 (PV_3)	125000 (PV_2, PV_3)
4	128000 (PV_2, PV_3 + Line 1-2, 2-3, 3-11)	127000 (PV_2, PV_3 + Line 1-2, 2-3)
8	128000 (PV_2, PV_3 + Line 1-2, 2-3, 3-11)	127000 (PV_2, PV_3 + Line 1-2, 2-3)
16	128000 (PV_2, PV_3 + line 1-2, 2-3, 3-11)	165000 (PV_2, PV_3, SG_2)
32	128000 (PV_2, PV_3 + line 1-2, 2-3, 3-11)	165000 (PV_2, PV_3, SG_2)
64	130000 (PV_2, PV_3 + line 1-2, 2-3, 3-4, 4-5, 5-6, 3-11)	167000 (PV_2, PV3, SG_2 + line 4-5, 5-6)
128	130000 (PV_2, PV_3 + line 1-2, 2-3, 3-4, 4-5, 5-6, 3-11)	167000 (PV_2, PV_3, SG_2 + line 4-5, 5-6)

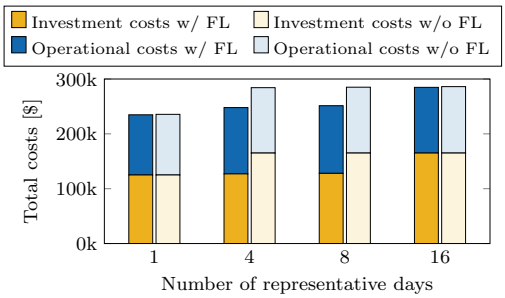

Fig. 7. Sensitivity of investment and operational costs to the presence of flexible loads for different representative days in Case 3.

leading to the intractability of the optimization problem as further clarified in Section IV-F. In particular, the results in Fig. 6 indicate that the overall costs plateau for excessive number of representative days, suggesting that the case studies considering up to 16 representative provide a good trade-off between the accuracy of cost estimates and the needed computational effort. Furthermore, Table VI provides the investment decisions for Cases 2 and 3. The additional units for the result of 16 and more representative days in Case 3, a consequence of the better representation of the operation scenarios further ensures that a more robust transient security solution is obtained.

2) Operational Flexibility: While flexible loads provide more degrees of freedom for operational planning, they are costly. In spite of their high operational costs, in this study they provide a more affordable option compared to investments in additional generators for improving system flexibility by reducing the peak power exchange with the main grid. Indeed, Table V shows a successive increase in the use of flexible loads for improving the transient frequency response. This is justified by the fact that flexible loads provide a peak shaving service vital for ensuring survivability during transients.

To this end, Case 3 was studied with and without flexible loads to thoroughly analyze their impact. In the case of 1 and 16 representative days, the operational costs experience a marginal decrease under the use of flexible loads, whereas the investment costs remain intact, as depicted in Fig. 7. In contrast, for other representative periods the use of flexible loads leads to lower investment costs, as they alleviate the problems pertaining to adequate power supply. Moreover, in all four cases the total costs increase without the use of flexible loads, thus making their adoption vital for system flexibility and economic operation. The latter aspect is primarily related to the presence of renewable PV units, which allow for the loads to be shifted to periods of higher solar generation. Note that the difference is more prominent in cases with 4 and 8 representative days since the use of flexible loads allows to differ investment decisions.

TABLE VII
COMPARISON BETWEEN OUT-OF-SAMPLE AND IN-SAMPLE TOTAL OPERATIONAL COSTS AND DESIGN FEASIBILITY

	Operational costs	Demand shift penalty	Demand disconnection penalty	Transient feasibility
Case 2	9.7% ↑	0.0%	0.0%	78.6%
Case 3	7.3% ↓	5.4% ↓	0.0%	100%

E. Out-of-sample Performance

To evaluate the performance of the system design and its feasibility against different realizations of uncertain parameters, we adopted the full pattern of realistic 365 days as out-of-sample scenarios for load and PV generation. Table VII presents a comparison between total operational costs of in-sample and out-of-sample scenarios. It is noteworthy to mention that in-sample scenarios are used within the proposed investment planning tool to obtain the optimal MG design, while the out-of-sample scenarios are used to evaluate the long-term performance of the optimal design under different realizations of uncertain loads and PV generations. Understandably, there is a slight increment in the total operational cost in Case 2 with only static security constraints. In other words, the stochastic approach may not be able to cover the entire spectrum of potential scenarios that may occur in system operation. However, the total costs with the inclusion of transient security constraints show a decrease indicating that the design remains robust to all different potential islanding scenarios in the year. Furthermore, Table VII shows the transient feasibility percentage for the optimal solutions in Case 2 and Case 3. According to Table VII, the optimal MG design in Case 2 is not feasible in 21.4% of the out-of-sample scenarios. However, the optimal design remains 100.0% feasible when considering either only static security or both static and transient security for MG design in Case 3. 0

F. Computational Effort and Scalability

All case studies have been performed on a laptop with an Intel Core i5 processor at 1.8GHz with 8GB memory. The three stages of the proposed algorithm are solved as: Stage 1 - stochastic-robust MILP; Stage 2 - deterministic Linear Programming (LP); and Stage 3 - analytical problem. For Stages 2 and 3, the computing time is less than 1.5 s on average to obtain the solution of each individual hour. However, in Stage 1, the solution space

TABLE VIII
COMPUTATION TIME FOR DIFFERENT REPRESENTATIVE DAYS

	Computation time [s]		
No. of representative days	GUROBI	CPLEX	MOSEK
1	25	26	28
4	63	108	274
8	156	230	689
16	354	465	2254
64	2787	6027	189658

of the problem is a function of the number of scenarios, i.e., number of representative days. In Table. VIII, a comparison of the computational time for different numbers of representative days and different state-of-the-art optimization tools is presented. An increase in the number of representative days leads to a larger solution space with more decision variables, and consequently, a higher computational time. By adopting a suitable solver, the computational time can be optimized. In Table. VIII GUROBI solver indicates the fastest response. Nonetheless, the exponential growth in solution time and increase in the solution space with the number of representative days can further increase the risk of intractability. Therefore, it is vital to compromise between accuracy and tractability of the proposed planning tool by choosing a sufficient number of representative days. In the same regard, a single-year planning model was utilized as opposed to a multi-year model. While the latter provides a higher accuracy, the number of variables and constraints increase significantly resulting in a higher risk of intractability.

V. CONCLUSION

MGs are expected to play a significant role in increasing the resilience of electric power systems. Their ability to operate in both grid-connected and islanded mode is paramount to their capacity to enhance system reliability. In this paper, the MG investment planning problem under both static and transient islanding constraints is investigated. By explicitly embedding the islanding constraints in the planning problem, the survivability of the system can be guaranteed and the resilience can be assessed as a function of the load supplied in islanded conditions. However, after the islanding event, the transient behavior of the MG is dictated both by the non-linear dynamics and the investment and operation decisions, which poses many challenges concerning the problem formulation. We tackle this problem by proposing an iterative three-stage algorithm that resolves the underlying tractability issues and computational challenges, as well as shows excellent performance on the examined case studies.

Nevertheless, several additional aspects still need to be investigated in ongoing and future work. For instance, the impact of information exchange between different layers of the algorithm on the solution optimality and rate of convergence need to be assessed. Furthermore, a trade-off between the accuracy of the transient response model of the MG and the model complexity should be considered. It is clear though that the need to consider system dynamics within the MG investment and operational decisions is crucial for ensuring system resilience.

APPENDIX A
FORMULATION OF THE FREQUENCY METRICS

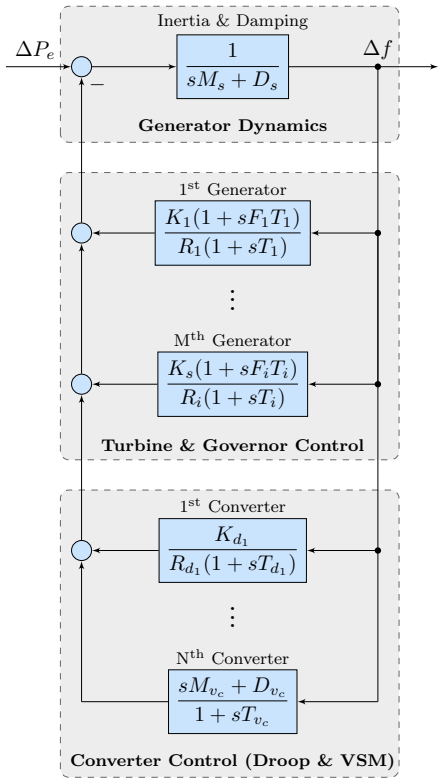

Fig. 8. Uniform system frequency dynamics model [23]

The detailed description of the frequency dynamics model adopted in this paper can be found in [31]. Here, a brief description on the formulation of the analytical model of the frequency metrics is presented.

The analytical model of the frequency metrics can be derived from the system frequency dynamic model illustrated in Fig. 8, for a system consisting of both CIGs and SGs. The transfer function $G(s)$ derived from Fig. 8 is given in (3). Based on the modeling assumptions defined in Section II-B, the transfer function is recast into (4), where the respective normalized parameters are defined as follows:

$$M_s = \sum_{i\in\Omega^{\mathrm{S}}} M_i \frac{P_i}{P_{b_s}}, \qquad D_s = \sum_{i\in\Omega^{\mathrm{S}}} D_i \frac{P_i}{P_{b_s}}, \tag{11a}$$

$$R_s = \sum_{i\in\Omega^{\mathrm{S}}} \frac{K_i}{R_i} \frac{P_i}{P_{b_s}}, \qquad F_s = \sum_{i\in\Omega^{\mathrm{S}}} \frac{K_i F_i}{R_i} \frac{P_i}{P_{b_s}}, \tag{11b}$$

$$M_c = \sum_{v\in\Omega_v^{\mathrm{C}}} M_v \frac{P_{c_v}}{P_{b_c}}, \qquad D_c = \sum_{v\in\Omega_v^{\mathrm{C}}} D_v \frac{P_{c_v}}{P_{b_c}}, \tag{11c}$$

$$R_c = \sum_{d\in\Omega_d^{\mathrm{C}}} R_d \frac{P_{c_d}}{P_{b_c}}, \qquad M = \frac{M_s P_{b_s} + M_c P_{b_c}}{P_{b_g} + P_{b_c}}, \tag{11d}$$

$$D = \frac{D_s P_{b_s} + D_c P_{b_c} + R_c P_{b_c}}{P_{b_s} + P_{b_c}}. \tag{11e}$$

Parameter P_i and P_c denotes the active power capacity of the SG and CIG, respectively, scaled over their respective sums of active power capacity of all connected SGs and CIGs, P_{b_s} and P_{b_c}. Note that the energy reserve capability for inertia and primary frequency response of CIG units is defined as function of the DC-side capacitor storage unit connected to the generator in this work. Therefore, the contribution of each CIG to the M and D

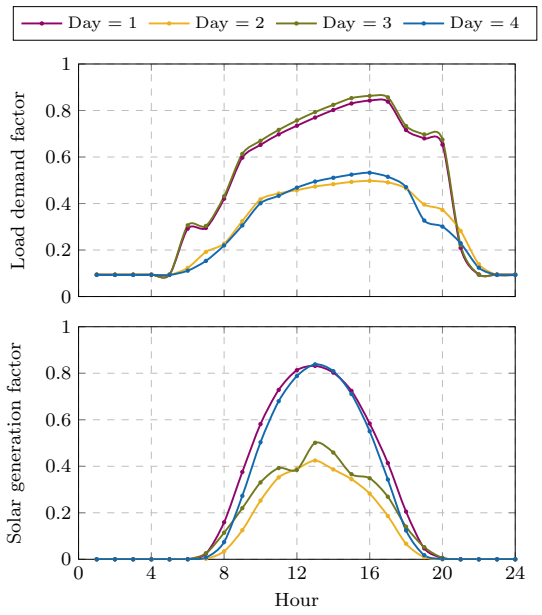

Fig. 9. Demand and solar power generation patterns (four representative days).

for frequency control was based on the capacity of the DC-side capacitor of associated unit [37].

By assuming a stepwise disturbance in the active power $\Delta P_e(s) = -\Delta P/s$, where ΔP is the net power change, the time-domain expression for frequency deviation ($\omega(t) \equiv \Delta f(t)$) can be derived as follows:

$$\omega(t) = -\frac{\Delta P}{M}\left(\frac{1}{T\omega_n^2} + \frac{1}{\omega_d}e^{-\zeta\omega_n t}\left(\sin\omega_d t - \frac{1}{\omega_n t}\sin\omega_d t + \phi\right)\right), \quad (12)$$

where $\omega_d = \omega_n\sqrt{1-\zeta^2}$ and $\phi = \sin^{-1}\left(\sqrt{1-\zeta^2}\right)$.

The RoCoF can be obtained by solving $\dot{\omega}(t)$, where the maximum RoCoF occurs at $t_r = 0^+$, i.e., $\dot{\omega}_{max} = \dot{\omega}(t_r)$, derived as indicated in (5a). The frequency nadir described in (5b) occurs at the time instance t_m when $\dot{\omega}(t_m) = 0$, whereas the quasi steady-state frequency given in (5c) is derived from (12) for $t \to \infty$.

Appendix B
Scenario Data

The profiles of four representative days for load and PV power generation are depicted in Fig. 9.

References

[1] S. S. M. Venkata and N. Hatziargyriou, "Grid resilience: Elasticity is needed when facing catastrophes [guest editorial]," *IEEE Power & Energy Magazine*, vol. 13, no. 3, pp. 16–23, May 2015.

[2] Y. Wang, C. Chen, J. Wang, and R. Baldick, "Research on resilience of power systems under natural disasters—a review," *IEEE Trans. Power Syst.*, vol. 31, no. 2, pp. 1604–1613, March 2016.

[3] A. Hussain, V.-H. Bui, and H.-M. Kim, "Microgrids as a resilience resource and strategies used by microgrids for enhancing resilience," *Applied Energy*, vol. 240, pp. 56 – 72, 2019.

[4] M. Panteli and P. Mancarella, "The grid: Stronger, bigger, smarter?: Presenting a conceptual framework of power system resilience," *IEEE Power and Energy Magazine*, vol. 13, no. 3, pp. 58–66, May 2015.

[5] "Ieee standard for the specification of microgrid controllers," *IEEE Std 2030.7-2017*, pp. 1–43, 2018.

[6] X. Liu, M. Shahidehpour, Z. Li, X. Liu, Y. Cao, and Z. Bie, "Microgrids for enhancing the power grid resilience in extreme conditions," *IEEE Trans. Smart Grid*, vol. 8, no. 2, pp. 589–597, March 2017.

[7] Y. Zhou, M. Panteli, R. Moreno, and P. Mancarella, "System-level assessment of reliability and resilience provision from microgrids," *Applied Energy*, vol. 230, pp. 374 – 392, 2018.

[8] F. Milano, F. Dörfler, G. Hug, D. J. Hill, and G. Verbič, "Foundations and challenges of low-inertia systems," in *2018 PSCC*, June 2018.

[9] W. Zheng, P. Crossley, B. Xu, and H. Qi, "Transient stability of a distribution subsystem during fault-initiated switching to islanded operation," *International Journal of Electrical Power & Energy Systems*, vol. 97, pp. 418 – 427, 2018.

[10] P. Kundur, J. Paserba, V. Ajjarapu, G. Andersson, A. Bose, C. Canizares, N. Hatziargyriou, D. Hill, A. Stankovic, C. Taylor, T. Van Cutsem, and V. Vittal, "Definition and classification of power system stability ieee/cigre joint task force on stability terms and definitions," *IEEE Transactions on Power Systems*, vol. 19, no. 3, pp. 1387–1401, 2004.

[11] E. Yamangil, R. Bent, and S. Backhaus, "Resilient upgrade of electrical distribution grids," in *29th AAAI Conf. on Artificial Intelligence*, 2015.

[12] A. Khodaei, S. Bahramirad, and M. Shahidehpour, "Microgrid planning under uncertainty," *IEEE Trans. Power Syst.*, vol. 30, no. 5, pp. 2417–2425, 2015.

[13] Y. Lin and Z. Bie, "Tri-level optimal hardening plan for a resilient distribution system considering reconfiguration and dg islanding," *Applied Energy*, vol. 210, pp. 1266 – 1279, 2018.

[14] S. Geng and M. Vrakopoulou and I. A. Hiskens, "Optimal Capacity Design and Operation of Energy Hub Systems," *Proceedings of the IEEE*, 2020.

[15] W. Yuan, J. Wang, F. Qiu, C. Chen, C. Kang, and B. Zeng, "Robust optimization-based resilient distribution network planning against natural disasters," *IEEE Trans. Smart Grid*, vol. 7, no. 6, pp. 2817–2826, 2016.

[16] S. Babaei, C. Zhao, and T. Ding, "Allocating distributed generators for resilient distribution system under uncertain probability distribution of natural disasters," in *2017 IEEE PES GM*, July 2017.

[17] R. Zarate-Minano, T. Van Cutsem, F. Milano, and A. J. Conejo, "Securing transient stability using time-domain simulations within an optimal power flow," *IEEE Trans. Power Syst.*, vol. 25, no. 1, pp. 243–253, Feb 2010.

[18] D. Gan, R. J. Thomas, and R. D. Zimmerman, "Stability-constrained optimal power flow," *IEEE Trans. Power Syst.*, vol. 15, no. 2, pp. 535–540, May 2000.

[19] P. Daly, D. Flynn, and N. Cunniffe, "Inertia considerations within unit commitment and economic dispatch for systems with high non-synchronous penetrations," in *2015 IEEE PowerTech*, June 2015.

[20] F. Teng, V. Trovato, and G. Strbac, "Stochastic scheduling with inertia-dependent fast frequency response requirements," *IEEE Trans. Power Syst.*, vol. 31, no. 2, pp. 1557–1566, 2016.

[21] S. S. Guggilam, C. Zhao, E. Dall'Anese, Y. C. Chen, and S. V. Dhople, "Optimizing der participation in inertial and primary-frequency response," *IEEE Trans. Power Syst.*, vol. 33, no. 5, pp. 5194–5205, 2018.

[22] H. Ahmadi and H. Ghasemi, "Security-constrained unit commitment with linearized system frequency limit constraints," *IEEE Trans. Power Syst.*, vol. 29, no. 4, pp. 1536–1545, July 2014.

[23] M. Paturet, U. Markovic, S. Delikaraoglou, E. Vrettos, P. Aristidou, and G. Hug, "Stochastic unit commitment in low-inertia grids," *IEEE Trans. Power Syst.*, pp. 1–1, 2020.

[24] X. Wu, Z. Wang, T. Ding, X. Wang, Z. Li, and F. Li, "Microgrid planning considering the resilience against contingencies," *IET Generation, Transmission Distribution*, vol. 13, no. 16, pp. 3534–3548, 2019.

[25] M. Mazidi, N. Rezaei, F. J. Ardakani, M. Mohiti, and J. M. Guerrero, "A hierarchical energy management system for islanded multi-microgrid clusters considering frequency security constraints," *Int. Journal of Elec. Power & Energy Sys.*, vol. 121, p. 106134, 2020.

[26] P. M. Anderson and M. Mirheydar, "A low-order system frequency response model," *IEEE Trans. Power Syst.*, vol. 5, no. 3, pp. 720–729, Aug 1990.

[27] S. Dehghan, N. Amjady, and P. Aristidou, "A robust coordinated expansion planning model for wind farm-integrated power systems with flexibility sources using affine policies," *IEEE Systems Journal*, 2019.

[28] M. E. Baran and F. F. Wu, "Network reconfiguration in distribution systems for loss reduction and load balancing," *IEEE Trans. Power Del.*, vol. 4, no. 2, pp. 1401–1407, April 1989.

[29] Z. Wang, B. Chen, J. Wang, J. Kim, and M. M. Begovic, "Robust optimization based optimal dg placement in microgrids," *IEEE Trans. Smart Grid*, vol. 5, no. 5, pp. 2173–2182, Sep. 2014.

[30] Z. Yang, H. Zhong, A. Bose, T. Zheng, Q. Xia, and C. Kang, "A linearized opf model with reactive power and voltage magnitude: A pathway to improve the mw-only dc opf," *IEEE Trans. Power Syst.*, vol. 33, no. 2, pp. 1734–1745, March 2018.

[31] U. Markovic, Z. Chu, P. Aristidou, and G. Hug, "LQR-Based Adaptive Virtual Synchronous Machine for Power Systems with High Inverter Penetration," *IEEE Trans. Sustain. Energy*, vol. 10, no. 3, pp. 1501–1512, July 2019.

[32] J. Rocabert, A. Luna, F. Blaabjerg, and P. Rodríguez, "Control of power converters in AC microgrids," *IEEE Trans. Power Electron.*, vol. 27, no. 11, pp. 4734–4749, Nov 2012.

[33] U. Markovic, O. Stanojev, P. Aristidou, and G. Hug, "Partial grid forming concept for 100% inverter-based transmission systems," in *2018 IEEE PES GM*, Aug 2018.

[34] U. Markovic, O. Stanojev, E. Vrettos, P. Aristidou, D. Callaway, and G. Hug, "Understanding Stability of Low-Inertia Systems," *IEEE Trans. Power Syst.*, (under review). [Online]. Available: engrxiv.org/jwzrq

[35] R. J.-B. Wets, "Stochastic programming models: Wait-and-see versus here-and-now." in *Decision Making Under Uncertainty. The IMA Volumes in Mathematics and its Applications*, vol. 128, 2002.

[36] European Commission, "Commission regulation (EU) 2016/631 of 14 april 2016 establishing a network code on requirements for grid connection of generators (RfG)," *Official Journal of the European Union*, 2016.

[37] U. Markovic, V. Häberle, D. Shchetinin, G. Hug, D. Callaway, and E. Vrettos, "Optimal sizing and tuning of storage capacity for fast frequency control in low-inertia systems," in *2019 International Conference on Smart Energy Systems and Technologies (SEST)*, 2019, pp. 1–6.

[38] Y. Wen, W. Li, G. Huang, and X. Liu, "Frequency dynamics constrained unit commitment with battery energy storage," *IEEE Transactions on Power Systems*, vol. 31, no. 6, pp. 5115–5125, 2016.

[39] R. Turvey and D. Anderson, *Electricity economics: Essays and case studies*. Johns Hopkins University Press, Baltimore, 1977.

[40] K. Strunz, E. Abbasi, R. Fletcher, N. Hatziargyriou, R. Iravani, and G. Joos, "Benchmark systems for network integration of renewable and distributed energy resources," *CIGRE Task Force C6.04.02*, 04 2014.

[41] U.S. Energy Information Administration, "Levelized costs of new generation resources in the annual energy outlook 2021," 2021. [Online]. Available: https://www.eia.gov/outlooks/aeo/pdf/electricity_generation.pdf

[42] Alliance for Sustainable Energy, Department of Energy (DOE), National Renewable Energy Laboratory (NREL), System Advisor Model, Version 2016.

[43] J. Löfberg, "Yalmip : A toolbox for modeling and optimization in matlab," in *2004 IEEE Intern. Conf. on Robotics and Automation*, 2004.

[44] L. Gurobi Optimization, "Gurobi optimizer reference manual," 2019.

[45] Kundur, P, Neal J. Balu, and Mark G. Lauby, *Power system stability and control*. New York: McGraw-Hill, 1994.

[46] "IEEE recommended practice for excitation system models for power system stability studies," *IEEE Std 421.5-2005 (Revision of IEEE Std 421.5-1992)*, pp. 1–93, 2006.

[47] P. Aristidou, S. Lebeau, and T. Van Cutsem, "Power system dynamic simulations using a parallel two-level schur-complement decomposition," *IEEE Trans. on Power Sys.*, vol. 31, no. 5, pp. 3984–3995, 2016.

Agnes Marjorie Nakiganda (S'15) received the B.Sc. degree in Electrical Engineering from the Makerere University, Uganda, in 2011. She obtained the M.Sc. degree in Electrical Engineering and Renewable Energy Systems in 2015 from the University of Leeds, Leeds, UK, where she is currently working towards the Ph.D. degree since October 2018. Her research interests include control and optimization of networks with a high penetration of converter-interfaced units.

Shahab Dehghan (S'08-M'14-SM'16) received the M.S. and Ph.D. degrees in Electrical Engineering from the Iran University of Science and Technology, Tehran, Iran, in 2009 and 2014, respectively. Currently, he is a researcher in at Imperial College London. His research interests include investment and operation planning in decarbonized power and energy systems.

Uros Markovic (S'16-M'20) was born in Belgrade, Serbia. He received the Dipl.-Eng. degree in Electrical Engineering from the University of Belgrade, Serbia, in 2013, with a major in power systems. He obtained the M.Sc. and Ph.D. degrees in Electrical Engineering and Information Technology in 2016 and 2020, respectively, both from the Swiss Federal Institute of Technology (ETH), Zurich, Switzerland. He is currently a joint Postdoctoral researcher with the Power Systems Laboratory and the Automatic Control Laboratory of ETH Zurich, Switzerland, and an affiliated researcher at the Grid Integration Group (GIG) of Lawrence Berkeley National Laboratory (LBNL), California, USA.

His research interests include power system dynamics, control and optimization, with a focus on stability and operation of inverter-dominated power systems with low rotational inertia.

Petros Aristidou (S'10-M'15-SM'20) received a Diploma in Electrical and Computer Engineering from the National Technical University of Athens, Greece, in 2010, and a Ph.D. in Engineering Sciences from the University of Liège, Belgium, in 2015. He is currently a Lecturer in Sustainable Power Systems at the Cyprus University of Technology. His research interests include power system dynamics, control, and simulation.

Gabriela Hug (S'05-M'08-SM'14) was born in Baden, Switzerland. She received the M.Sc. degree in electrical engineering in 2004 and the Ph.D. degree in 2008, both from the Swiss Federal Institute of Technology (ETH), Zurich, Switzerland. After the Ph.D. degree, she worked in the Special Studies Group of Hydro One, Toronto, ON, Canada, and from 2009 to 2015, she was an Assistant Professor in Carnegie Mellon University, Pittsburgh, PA, USA. She is currently an Associate Professor in the Power Systems Laboratory, ETH Zurich. Her research is dedicated to control and optimization of electric power systems.